Quantum nature of the hydrogen bond

Xin-Zheng Li, Brent Walker, and Angelos Michaelides[1]

London Centre for Nanotechnology and Department of Chemistry, University College London, London WC1E 6BT, United Kingdom

Hydrogen bonds are weak, generally intermolecular bonds, which hold much of soft matter together as well as the condensed phases of water, network liquids, and many ferroelectric crystals. The small mass of hydrogen means that they are inherently quantum mechanical in nature, and effects such as zero-point motion and tunneling must be considered, though all too often these effects are not considered. As a prominent example, a clear picture for the impact of quantum nuclear effects on the strength of hydrogen bonds and consequently the structure of hydrogen bonded systems is still absent. Here, we report ab initio path integral molecular dynamics studies on the quantum nature of the hydrogen bond. Through a systematic examination of a wide range of hydrogen bonded systems we show that quantum nuclear effects weaken weak hydrogen bonds but strengthen relatively strong ones. This simple correlation arises from a competition between anharmonic intermolecular bond bending and intramolecular bond stretching. A simple rule of thumb is provided that enables predictions to be made for hydrogen bonded materials in general with merely classical knowledge (such as hydrogen bond strength or hydrogen bond length). Our work rationalizes the influence of quantum nuclear effects, which can result in either weakening or strengthening of the hydrogen bonds, and the corresponding structures, across a broad range of hydrogen bonded materials. Furthermore, it highlights the need to allow flexible molecules when anharmonic potentials are used in force field-based studies of quantum nuclear effects.

Hydrogen bonds are essential to life on earth. They are, for example, the main intermolecular interactions responsible for binding the two strands of DNA and holding together the condensed phases of water. H-bonds are also of great contemporary importance in nanoscience, being involved in, e.g., the functionalization and patterning of surfaces with ordered molecular overlayers (1, 2). It is known that H-bonds are complex and, in particular, because of the small mass of the proton it is often not appropriate to treat the proton in H-bonded systems as a classical particle. Instead the quantum nature of the proton must be taken into account and issues such as zero-point motion, quantum delocalization, and quantum tunneling are relevant. Recent advances in experimental techniques and the development of theoretical approaches (coupled with enormous advances in computer power) mean it is now possible to explore the quantum nature of the proton in H-bonded systems in exquisite detail. The relevance of quantum nuclear effects (QNEs) to liquid water and ice (3–8), interfacial water (9), and enzyme kinetics (10, 11) has recently been demonstrated. In particular, from first principles simulations by Morrone et al. (4, 12) and neutron Compton scattering measurements by Burnham et al. (13, 14), a clear picture of the impact of QNEs on the proton's real space delocalization and vibrational properties has been established. Upon increasing the H-bond strength, the proton becomes more delocalized and consequently the OH stretching frequency decreases.

QNEs can also influence the interaction strength and consequently the structure of H-bonded systems (4, 8, 9, 15–19). In H-bonded crystals, this effect is known as the Ubbelohde effect, where replacing H with deuterium (D) causes the O-O distance, and consequently the ferroelectric phase-transition temperature, to change (20). The conventional Ubbelohde effect yields an elongation of the O-O distances upon replacing H with D,

although a negative Ubbelohde effect has also been observed (20, 21). In H-bonded liquids analogous issues have been discussed. In liquid hydrogen fluoride (HF), for example, density-functional theory (DFT) simulations predict that when QNEs are accounted for the first peak of the F-F radial distribution function (RDF) sharpens and shifts to a shorter F-F distance (15). The implication of this increase in structure in the liquid is that the H-bond is strengthened upon inclusion of QNEs. In contrast, similar simulations for liquid water show that the O-O RDF is less sharply peaked when simulations with quantum nuclei are compared to those with classical nuclei (4), suggestive of a decrease in the overall H-bond strength. We note, however, that although this conclusion is probably correct, it is the opposite of what was observed in an earlier ab initio study (8). The influence of QNEs on H-bonds has also been widely discussed in studies of gas-phase clusters (16–18, 22). Specifically, in water clusters up to the hexamer it is predicted that QNEs weaken the H-bonds, whereas in simulations of HF clusters both weakening and strengthening is predicted depending on cluster size (16–18). Clearly, it would be very useful to rationalize these various results within a single conceptual framework and identify the underlying factors that dictate the influence of QNEs on H-bond strength for a broad class of materials.

To this end, we report herein a simulation study in which we investigate the impact of QNEs on a wide range of H-bonded materials. Our simulations, using state-of-the-art ab initio molecular dynamics (MD) and ab initio path integral molecular dynamics (PIMD) [see, e.g., (23–27)], reveal that the strength of the H-bond is a good descriptor of what influence QNEs will have on it: Relatively weak H-bonds, such as those in water and HF dimers, are made weaker, whereas relatively strong H-bonds, such as those in large HF clusters and certain solids, are made stronger by QNEs. This correlation holds for a large variety of hydrogen-bonded systems and arises from a simple competition between the anharmonic quantum fluctuations of intramolecular covalent bond stretching (which tends to strengthen H-bonds) and intermolecular H-bond bending (which tends to weaken H-bonds). It has a number of important implications, such as explaining the contrasting influence QNEs have on a wide range of H-bonded materials and enabling predictions to be made for H-bonded materials in general. Since the extent of anharmonic quantum motion on intramolecular stretching is key to the correlation, it also underscores the need for flexible monomers when anharmonic intermolecular potentials are used in force field-based studies of QNEs.

Results

Toward our aim of understanding how QNEs alter H-bonds, we use computer simulations with the CASTEP plane-wave DFT code (28). The simulations are performed with the Perdew–Burke–Ernzerhof (PBE) exchange-correlation functional (29) in the canonical ensemble, with a target temperature of 100 K.

Further computational details are given in *Materials and Methods* below.

A broad range of H-bonded systems are examined, including HF clusters (dimer to hexamer), H_2O clusters (dimer, pentamer, and octamer); charged, protonated, and hydroxylated water and ammonia clusters ($H_9O_5^-$, $H_9O_4^+$, $H_7O_4^-$, and $N_2H_5^-$); organic dimers (formic acid and formamide); and solids (HF, HCl, and squaric acid $C_4H_2O_4$). For each system we perform conventional ab initio MD, where the nuclei are treated as classical point-like particles, and ab initio PIMD, where the QNEs are accounted for. With these two complementary sets of simulations, we can identify in a very clean manner the precise influence of QNEs at finite temperature.

The quantities we focus on when characterizing H-bonds are: (*i*) the heavy-atom (X-X, where X is either O, Cl, C, N, or F) distances, which characterize the intermolecular separations; (*ii*) the H-bond angles (X-H...X), which are associated with H-bond bending (libration) modes; and (*iii*) the X-H covalent bond lengths, characteristic of the covalent bond stretching in the H-bond donor molecules. It will become clear that these quantities provide an indication of H-bond strength, however, as the main measure of H-bond strength we use a standard estimate based on the computed redshift (softening) in the X-H stretching frequency of the H-bond donor molecule (*Materials and Methods*). In fact, there is no perfect measure for H-bond strength (30), however the redshift of the stretching frequency is a widely used measure [see, e.g., (31, 32)]. It is particularly useful here because it allows us to discriminate between different types of H-bond in the same complex and can be used for both neutral and charged systems. In Fig. 1*B*, it is shown that this estimator correlates well with the computed binding energy per H-bond in the neutral systems we study. This binding energy is defined as the difference between the total energy of the system and the sum over its unrelaxed components, as in ref. 30. When the redshift of the stretching frequency (measured as the ratio of the X-H stretching frequency in the H-bonded cluster to that in the free monomer) gets larger, the H-bond comes stronger.

Upon comparing the results from MD and PIMD for the various H-bonded systems, an interesting correlation is observed between H-bond strength and the change in intermolecular separations. This correlation is shown in Fig. 1*A* where we see that as the H-bond gets stronger the heavy-atom separations in the PIMD simulations with quantum nuclei go from being longer than those in the MD simulations with classical nuclei (positive $\Delta(X - X)$) to being shorter (negative $\Delta(X - X)$). Thus QNEs result in longer H-bonds in weak H-bonded systems and shorter H-bonds in relatively strong H-bonded systems. Note that the H-bond strength increases upon going from small to large clusters and from water to HF. The trend reported in Fig. 1 is a key finding of the present study and in the following we explain why it emerges and discuss the implications it has for H-bonded materials in general.

To understand the origin of the correlation it is useful to look at the HF clusters. These provide the ideal series because upon increasing the cluster size the H-bond strength increases, and the influence of QNEs switches from a tendency to lengthen to a tendency to shorten the intermolecular separations (as seen in ref. 16). In Fig. 2 we report distance and angle distributions from MD and PIMD for three HF clusters: the dimer, in which the F-F distance is increased by QNEs; the tetramer, where there is no difference between the quantum and classical F-F distances; and the pentamer, where the F-F distance is shortened by QNEs. The key to understanding the variations in heavy-atom distances (*Left*) is in recognizing that there are also related differences between MD and PIMD in the covalent F-H bond lengths (*Center*) and H-bond angles (*Right*). Specifically, because of anharmonic quantum fluctuations (*i*) the F-H bonds are longer in the quantum compared to the classical simulations, and this elongation
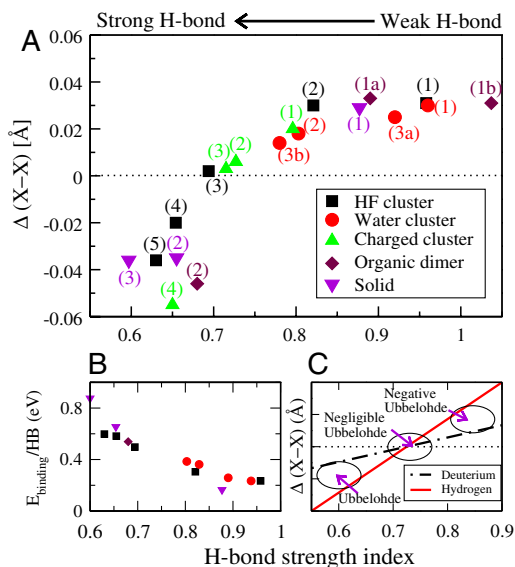

Fig. 1. (*A*) Differences between the shortest heavy-atom distances from PIMD and MD simulations [$(X − X)^{PIMD}_{average} − (X − X)^{MD}_{average}$, denoted by $\Delta(X − X)$], vs. H-bond strength (defined as the ratio of the X-H stretching frequency in the H-bonded cluster to that in the free monomer). (*B*) Correlation between this H-bond strength index and the binding energy per H-bond in the neutral systems considered. (*C*) Simplified schematic illustration of the expected isotope (Ubbelohde) effect on the differences in heavy-atom distances. Here we suggest three regimes of positive, negligible, and negative Ubbelohde effect depending on H-bond strength. For the HF clusters, labels 1–5 refer to the H-bonds in the dimer to the hexamer. For the water clusters, labels 1, 2, 3a, and 3b refer to the H-bonds in the dimer, pentamer, and the long (short) H-bond in the octamer. For the charged clusters, labels 1–4 refer to $H_9O_5^-$, $H_9O_4^+$, $H_7O_4^-$, and $N_2H_5^-$, respectively. For the organic dimers, labels 1a, 1b, and 2 refer to the redshifted and blueshifted H-bond in formamide and the redshifted H-bond in formic acid. For the solids, labels 1–3 refer to the H-bonds in HCl, HF, and squaric acid. The same labels are applied in Fig. 3. For the water clusters in *B*, the octamer is not included because there are two kinds of H-bonds. Results for the trimer and tetramer are added to further test the correlation.

becomes more pronounced as the H-bonds get stronger; and (*ii*) the H-bonds are more bent in the quantum than in the classical simulations, and this bending generally becomes less pronounced as the H-bonds get stronger. In order to understand the influence of these variations in structure, analysis of various dimer configurations is performed. This analysis reveals that the covalent bond stretching increases the intermolecular interaction whereas H-bond bending decreases it. Taking the HF dimer as an example, a 0.04-Å increase in the F-H bond length of the donor leads to a 40-meV increase in interaction energy within the dimer, whereas in contrast a 21° reduction in H-bond angle leads to a 16-meV decrease in interaction energy. These considerations provide a qualitative understanding of the trend observed. In the HF dimer the F-F distance increases as a result of a large decrease in H-bond angle but only a small increase in the covalent F-H bond length. In the tetramer, the F-H stretching is sufficiently pronounced to compensate for the increase in H-bond bending, leaving the overall F-F distance unchanged and in the pentamer, the F-F distance decreases because the F-H covalent bond stretching dominates over the H-bond bending.

To examine this picture rigorously and present a quantitative description of this competition for all systems studied, we calculate the projection $(X − H^{\parallel})$ of the donor molecule's covalent bond along the intermolecular axis (see inset of Fig. 3). Since $X − H^{\parallel}$ increases upon intramolecular stretching but decreases upon intermolecular bending, it allows the balance between stretching and bending to be evaluated. The influence of QNEs is quantified through the ratio of the PIMD and MD projections,
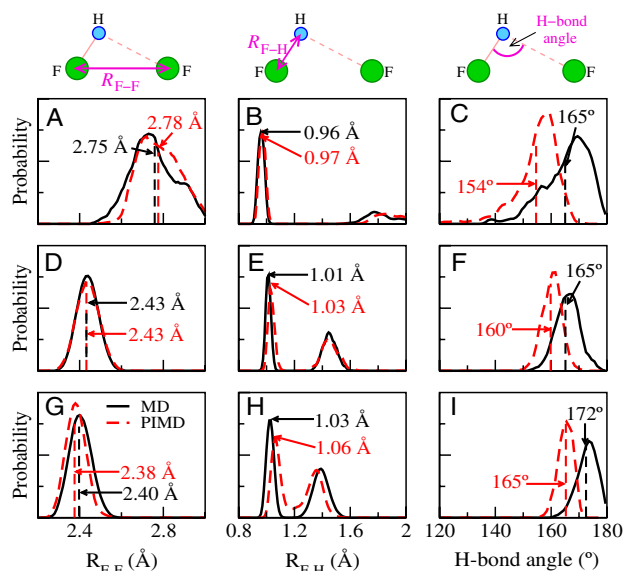
Li et al.

Fig. 2. Distributions of the F-F distances (*Left*), the F-H bond lengths (*Center*), and the intermolecular bending (F-H···F angle, *Right*) from MD (solid black lines) and PIMD (dashed red lines) for a selection of systems: the HF dimer (*Top*), the HF tetramer (*Middle*), and the HF pentamer (*Bottom*). The MD and PIMD averages are shown in black and red, respectively.

$x = (X - H^{\parallel})^{PIMD}/(X - H^{\parallel})^{MD}$; values greater than one indicate that QNEs lead to more stretching than bending and values less than one indicate that QNEs result in more bending than stretching. Upon plotting this ratio against the variations in intermolecular separations, $y = \Delta(X - X)$, we observe a striking (almost linear) correlation (Fig. 3). We see that for all systems where H-bond bending dominates (x clearly smaller than 1), the heavy-atom distances are longer in PIMD than in MD ($y > 0$). In cases where covalent bond stretching is dominant (x clearly larger than 1), the heavy-atom distances are shorter in PIMD than in MD ($y < 0$). With the increase of x, quantum fluctuations on the stretching mode become more dominant and QNEs turn from weakening the H-bonds to strengthening them. Thus the overall
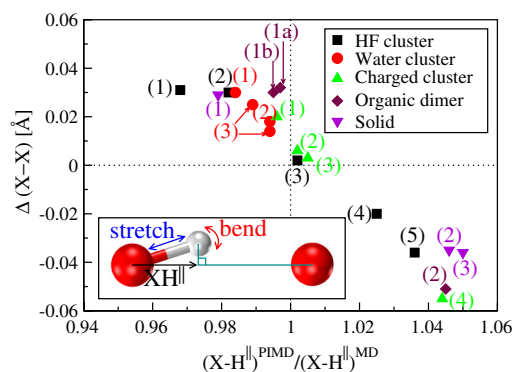

Fig. 3. Differences in average shortest heavy-atom distances between PIMD and MD simulations ($\Delta(X - X)$, vertical axis) vs. the ratio of the projection of the donor X-H covalent bond along the intermolecular axis from PIMD and MD simulations (horizontal axis). For the meaning of the labels please refer to the caption of Fig. 1. Large (small) x indicates a dominant contribution from the stretching (bending) mode due to quantum fluctuations. Negative values of $\Delta(X - X)$ indicate that QNEs decrease the intermolecular separation. An almost linear correlation between the two variables can be observed: When the contribution from stretching becomes more dominant, the QNEs turn from weakening to strengthening the H-bonds. The inset illustrates the geometry used for projecting the donor covalent X-H bond onto the intermolecular axis. The curved red arrow represents the intermolecular bending and the straight blue arrow represents the intramolecular stretching.

influence of QNEs on the H-bonding interaction quantitatively comes down to this delicate interplay between covalent bond stretching and intermolecular bond bending. We note that the explanation arrived at here for the general case is consistent with what Manolopoulos and coworkers have very elegantly shown for liquid water (6).

Discussion

Given the ubiquity of H-bonds in the physical and biological sciences, there are a number of implications of this work. First, considering that liquid HF is comprised of long polymer chains and rings whereas liquid water is widely considered to be made up of small clusters, these results shed light on why QNEs strengthen the structure of liquid HF but weaken that of liquid water (4). More generally, we can use the trend observed in Fig. 1 as a simple rule of thumb to estimate the impact of QNEs on H-bonded systems without performing expensive PIMD simulations. All that is required is an estimate of H-bond strength, which can be obtained from the redshift in the covalent stretching frequency (as we have done here) or from other commonly used measures of H-bond strength such as H-bond length. Thus the trend may be particularly useful to biological systems such as alpha helixes and beta sheets for which many crystal structures have been determined and where cooperative effects lead to particularly strong H-bonds (33).

The trend predicted here also allows us to rationalize the Ubbelohde effect over a broad range of H-bond regimes (Fig. 1C). Specifically, traditional Ubbelohde ferroelectrics such as potassium dihydrogen phosphate fall in the relatively strong H-bond regime where a positive Ubbelohde effect (i.e., an increase of the X-X distance upon replacing H with D) is observed in experiment and also in recent PIMD studies (21, 34). In this context squaric acid, solid HF, and the larger HF clusters are expected to exhibit a traditional Ubbelohde effect upon replacing H with D. In contrast, the smaller H-bonded clusters studied here and solid HCl are expected to exhibit a negative Ubbelohde effect (a decrease of the X-X distance upon replacing H with D). H-bonded materials of intermediate strength such as large water clusters and ice at ambient pressure are predicted to exhibit a negligible Ubbelohde effect because in this regime QNEs have little influence on the intermolecular separations. Indeed this observation is consistent with experimental and theoretical observations for the ferroelectric H-bonded crystals, ice, and gas-phase dimers (20–22). We note that we have considered the "fm2" configuration of the formamide organic dimer (33), which has a blueshifted H-bond (as well as a redshifted one); the data in this case also agrees with the correlation we observe for the other H-bonded systems (Fig. 1A).

A further prediction stemming from our work is that ice under pressure will exhibit the traditional Ubbelohde effect. However we caution that at very high pressure ice possesses such strong H-bonds, with shared symmetric protons (7), that the picture sketched in Fig. 3 is not likely to apply. Indeed, this note of caution applies to all ultrastrong H-bonds, where the proton is shared symmetrically by the two heavy atoms already in the classical perspective. In this case, the distinction between a relatively short covalent bond and a relatively long H-bond is lost and bond stretching along the X-X axis does not lead to any strengthening of the intermolecular interactions. The gas-phase Zundel complex, $H_5O_2^+$, is an example of one such ultrastrong H-bond and our calculations show an approximately 0.016-Å increase in the O-O distance, which is consistent with previous studies (27, 35). Another class of very strong H-bonded systems are the so-called "low-barrier" H-bonds, e.g., $H_3O_2^-$, $N_2H_7^+$, and $N_2H_5^-$. In these systems there remains a clear distinction between covalent and H-bonds and the picture we have presented still holds. This fact can be seen from our data for $N_2H_5^-$ in Fig. 1. We caution, however, that in these very strong H-bonded systems errors associated

with the underlying exchange-correlation functional can have a qualitative impact on the results and that the accuracy of the underlying potential energy surface is of critical importance. For example, in $H_3O_2^-$ and $N_2H_7^+$, using the PBE exchange-correlation functional yields a shared symmetric proton already in the classical MD simulations. But earlier studies with the more accurate second-order Møller–Plesset perturbation theory and also the Becke–Lee–Yang–Parr exchange-correlation functional (27, 35, 36) show that protons actually feel a double-well potential and in this case QNEs strengthen the H-bond, consistent with the model presented here.

Finally, because both inter- and intramolecular vibrations are relevant to QNEs, this work highlights the need in general for flexible monomers in force-field simulations of QNEs, as was also pointed out recently for liquid water (6). If such simulations do not allow for covalent bond stretching within the H-bond donor molecule, it appears that nothing but H-bond weakening will be observed upon inclusion of QNEs. Similarly if librations are neglected in studying QNEs on H-bonds (e.g., when linear H-bond models are used), nothing but H-bond strengthening can be expected. Indeed, this observation is consistent with an earlier study on H-bonded dimers using a model Hamiltonian, where it was found that without considering the zero-point energy on the bending mode, negative Ubbelohde effects cannot be explained (22).

In conclusion, through a series of ab initio MD and PIMD studies, light has been shed on the quantum nature of the H-bond. The impact of the quantum mechanics of the nuclei on the nature and strength of H-bonds has been widely discussed. However, such discussions have generally been on a case by case basis and a theoretical framework that rationalizes the different behavior observed in liquids, solids, and clusters has been lacking. Here we have identified H-bond strength as a simple descriptor, which shows that relatively weak H-bonds such as those in water and HF dimers and solid HCl are made weaker, whereas relatively strong H-bonds with a double-well potential for the proton transfer, such as those in large HF clusters, solid HF, and squaric acid, are made stronger. It remains to be seen how far the simple trend identified here can be extended and what exceptions will arise in addition to the ultrastrong H-bonded systems. However, it is clear that the identification of this relation brings physical insight and enables predictions to be made for a broad range of H-bonded systems, based merely on easily accessible quantities, such as vibrational frequencies or heavy-atom separations.

Materials and Methods

Born–Oppenheimer MD simulations are performed with a plane-wave basis set (kinetic energy cutoff 400 eV) in conjunction with ultrasoft pseudopotentials (37). For the water and HF clusters, a 12-Å cubic cell is used. For the organic dimers and charged water clusters, an 18-Å cubic cell is used. For the formamide dimer, we use the fm2 structure of ref. 33, where there is one redshifted H-bond and one blueshifted H-bond. For solid HF and HCl we use an eight molecule supercell with a $4 \times 2 \times 3$ Monkhorst–Pack k-point mesh. For solid squaric acid, we use a 20-atom cell with a $3 \times 3 \times 2$ Monkhorst–Pack k-point mesh. Timesteps of 0.5–0.7 fs are used and after thermal equilibration 10,000 MD steps and 6,000 PIMD steps are performed. In the PIMD simulations 16 beads and staging coordinates (38) are used. Convergence with respect to the number of beads was checked by performing calculations for the water dimer with 32 and 64 beads. All MD and PIMD simulations are performed at a target temperature of 100 K, except in solid HCl ($N_2H_5^-$), where 50 (300) K is used to keep the system close to the ground state (to compare with earlier calculations). Temperatures are maintained by Langevin thermostats. All the PIMD distances reported are obtained by averaging over configurations of the individual beads; using centroids gives the same correlation as shown in the article.

To calculate the redshift in the X-H vibrational frequency, we extract harmonic frequencies using finite displacements about the optimized geometries. This method provides a reasonable estimate of the frequency, and it is free of the deficiency in the path integral based approaches, like centroid molecular dynamics (39) and ring-polymer molecular dynamics (40), especially at low temperatures, as recently pointed out in refs. 41 and 42.

1. Barth JV, Costantini G, Kern K (2005) Engineering atomic and molecular nanostructures at surfaces. *Nature* 437:671–679.
2. Grimsdale AC, Mullen K (2005) The chemistry of organic nanomaterials. *Angew Chem Int Ed* 44:5592–5629.
3. Marx D, Tuckerman ME, Hutter J, Parrinello M (1999) The nature of the hydrated excess proton in water. *Nature* 397:601–604.
4. Morrone JA, Car R (2008) Nuclear quantum effects in water. *Phys Rev Lett* 101:017801.
5. Fanourgakis GS, Schenter GK, Xantheas SS (2006) A quantitative account of quantum effects in liquid water. *J Chem Phys* 125:141102.
6. Habershon S, Markland TE, Manolopoulos DE (2009) Competing quantum effects in the dynamics of a flexible water model. *J Chem Phys* 131:024501.
7. Benoit M, Marx D, Parrinello M (1998) Tunneling and zero-point motion in high-pressure ice. *Nature* 392:258–261.
8. Chen B, Ivanov I, Klein ML, Parrinello M (2003) Hydrogen bonding in water. *Phys Rev Lett* 91:215503.
9. Li XZ, Probert MIJ, Alavi A, Michaelides A (2010) Quantum nature of the proton in water-hydroxyl overlayers on metal surfaces. *Phys Rev Lett* 104:066102.
10. Masgrau L, et al. (2006) Atomic description of an enzyme reaction dominated by proton tunneling. *Science* 312:237–241.
11. Truhlar DG (2010) Tunneling in enzymatic and nonenzymatic hydrogen transfer reactions. *J Phys Org Chem* 23:660–676.
12. Morrone JA, Lin L, Car R (2009) Tunneling and delocalization effects in hydrogen bonded systems: A study in position and momentum space. *J Chem Phys* 130:204511.
13. Burnham CJ, et al. (2006) On the origin of the redshift of the OH stretch in Ice Ih: Evidence from the momentum distribution of the protons and the infrared spectral density. *Phys Chem Chem Phys* 8:3966–3977.
14. Burnham CJ, et al. (2008) The vibrational proton potential in bulk liquid water and ice. *J Chem Phys* 128:154519.
15. Raugei S, Klein ML (2003) Nuclear quantum effects and hydrogen bonding in liquids. *J Am Chem Soc* 125:8992–8993.
16. Swalina C, Wang Q, Chakraborty A, Hammes-Schiffer S (2007) Analysis of nuclear quantum effects on hydrogen bonding. *J Phys Chem A* 111:2206–2212.
17. Gregory JK, Clary DC (1996) Structure of water clusters. The contribution of many-body forces, monomer relaxation, and vibrational zero-point energy. *J Phys Chem* 100:18014–18022.
18. Clary DC, Benoit DM, Van Mourik T (2000) H-densities: A new concept for hydrated molecules. *Acc Chem Res* 33:441–447.
19. Morrone JA, Srinivasan V, Sebastiani D, Car R (2007) Proton momentum distribution in water: An open path integral molecular dynamics study. *J Chem Phys* 126:234504.
20. Ubbelohde AR, Gallagher KJ (1955) Acid-base effects in hydrogen bonds in crystals. *Acta Crystallogr* 8:71–83.
21. Matsushita E, Matsubara T (1982) Note on isotope effect in hydrogen bonded crystals. *Prog Theor Phys* 67:1–19.
22. Legon AC, Millen DJ (1988) Systematic effect of D substitution on hydrogen-bond lengths in gas-phase dimers B…HX and a model for its interpretation. *Chem Phys Lett* 147:484–489.
23. Marx D, Parrinello M (1994) Ab initio path integral molecular dynamics. *Z Phys B Condens Matter* 95:143–144.
24. Marx D, Parrinello M (1995) Structural quantum effects and 3-center 2-electron bonding in CH5+. *Nature* 375:216–218.
25. Marx D, Parrinello M (1996) Ab initio path integral molecular dynamics: Basic ideas. *J Chem Phys* 104:4077–4082.
26. Tuckerman ME, Marx D, Klein ML, Parrinello M (1996) Efficient and general algorithms for path integral Car–Parrinello molecular dynamics. *J Chem Phys* 104:5579–5588.
27. Tuckerman ME, Marx D, Klein ML, Parrinello M (1997) On the quantum nature of the shared proton in hydrogen bonds. *Science* 275:817–820.
28. Clark SJ, et al. (2005) First principles methods using CASTEP. *Z Kristallogr* 220:567–570.
29. Perdew JP, Burke K, Ernzerhof M (1996) Generalized gradient approximation made simple. *Phys Rev Lett* 77:3865–3868.
30. Wendler K, Thar J, Zahn S, Kirchner B (2010) Estimating the hydrogen bond energy. *J Phys Chem A* 114:9529–9536.
31. Xantheas SS, Dunning TH (1993) Ab-initio studies of cyclic water clusters $(H_2O)_N$, $N = 1–6$. 1. Optimal structures and vibrational spectra. *J Chem Phys* 99:8774–8792.
32. Cubero E, Orozco M, Hobza P, Luque FJ (1999) Hydrogen Bond versus Anti-Hydrogen Bond: A Comparative Analysis Based on the Electron Density Topology. *J Phys Chem A* 103:6394–6401.
33. Ireta J, Neugebauer J, Scheffler M, Rojo A, Galvan MJ (2003) Density functional theory study of the cooperativity of hydrogen bonds in finite and infinite alpha-helices. *J Phys Chem B* 107:1432–1437.
34. Srinivasan V, Car R, Sebastiani D (2010) The isotope-effect in the phase transition of KDP: New insights from ab initio path integral simulations. arXiv:10021457.

35. Tachikawa M, Shiga M (2005) Geometrical H/D isotope effect on hydrogen bonds in charged water clusters. *J Am Chem Soc* 127:11908–11909.

36. Ishibashi H, Hayashi A, Shiga M, Tashikawa M (2008) Geometrical isotope effect on the $N_2H_7^+$ cation and $N_2H_5^-$ anion by ab initio path integral molecular dynamics simulation. *ChemPhysChem* 9:383–387.

37. Vanderbilt D (1990) Soft self-consistent pseudopotentials in a generalized eigenvalue formalism. *Phys Rev B Condens Matter Mater Phys* 41:7892–7895.

38. Tuckerman ME, Berne BJ, Martyna GJ, Klein ML (1993) Efficient molecular-dynamics and hybrid Monte-Carlo algorithms for path integrals. *J Chem Phys* 99:2796–2808.

39. Voth GA (1996) Path integral centroid methods in quantum statistical mechanics and dynamics. *Adv Chem Phys* 93:135–218.

40. Craig IR, Manolopoulos DE (2004) Quantum statistics and classical mechanics: Real time correlation functions from ring polymer molecular dynamics. *J Chem Phys* 121:3368–3373.

41. Witt A, et al. (2009) On the applicability of centroid and ring polymer path integral molecular dynamics for vibrational spectroscopy. *J Chem Phys* 130:194510.

42. Ivanov SD, et al. (2010) Communications: On artificial frequency shifts in infrared spectra obtained from centroid molecular dynamics: Quantum liquid water. *J Chem Phys* 132:031101.

CHEMISTRY